Supplemental Information

LRP-1 Links Post-Translational Modifications to Efficient Presentation of Celiac Disease-Specific T Cell Antigens

Elise Loppinet[1], Harrison A. Besser[2,3], Agnele Sylvia Sewa[4], Fu-Chen Yang[2], Bana Jabri[5], Chaitan Khosla[1,2,6,]*

[1]Department of Chemical Engineering, Stanford University, Stanford, CA 94305, USA.
[2]Department of Chemistry, Stanford University, Stanford, CA 94305, USA.
[3]Stanford Medical Scientist Training Program, Stanford University School of Medicine, Stanford, CA 94305, USA.
[4]Department of Biochemistry, Stanford University School of Medicine, Stanford, CA 94305, USA.
[5]Department of Medicine, University of Chicago, Chicago, IL 60637, USA.
[6]Sarafan ChEM-H, Stanford University, Stanford, CA 94305, USA.
*Corresponding author: khosla@stanford.edu

Figure S1: Inhibition kinetics of HB225 and HB230 and wide panel views of panels in Fig. 1: (A) Comparison of TG2 inhibition by HB225 and HB230. The two compounds have very similar kinetic properties. Data are represented as mean ± SD. (B) Treatment with RZ-5 results in puncta similar to those seen using HB230. Wide view images of cells in Fig. 1. (C) HB230 (D) HB230 in TG2 knock out MEFs (E) 5BP (E) Cells pre-treated with CK805. (G) TG2 staining in live (top) and fixed (bottom) cells. Related to Fig. 1.

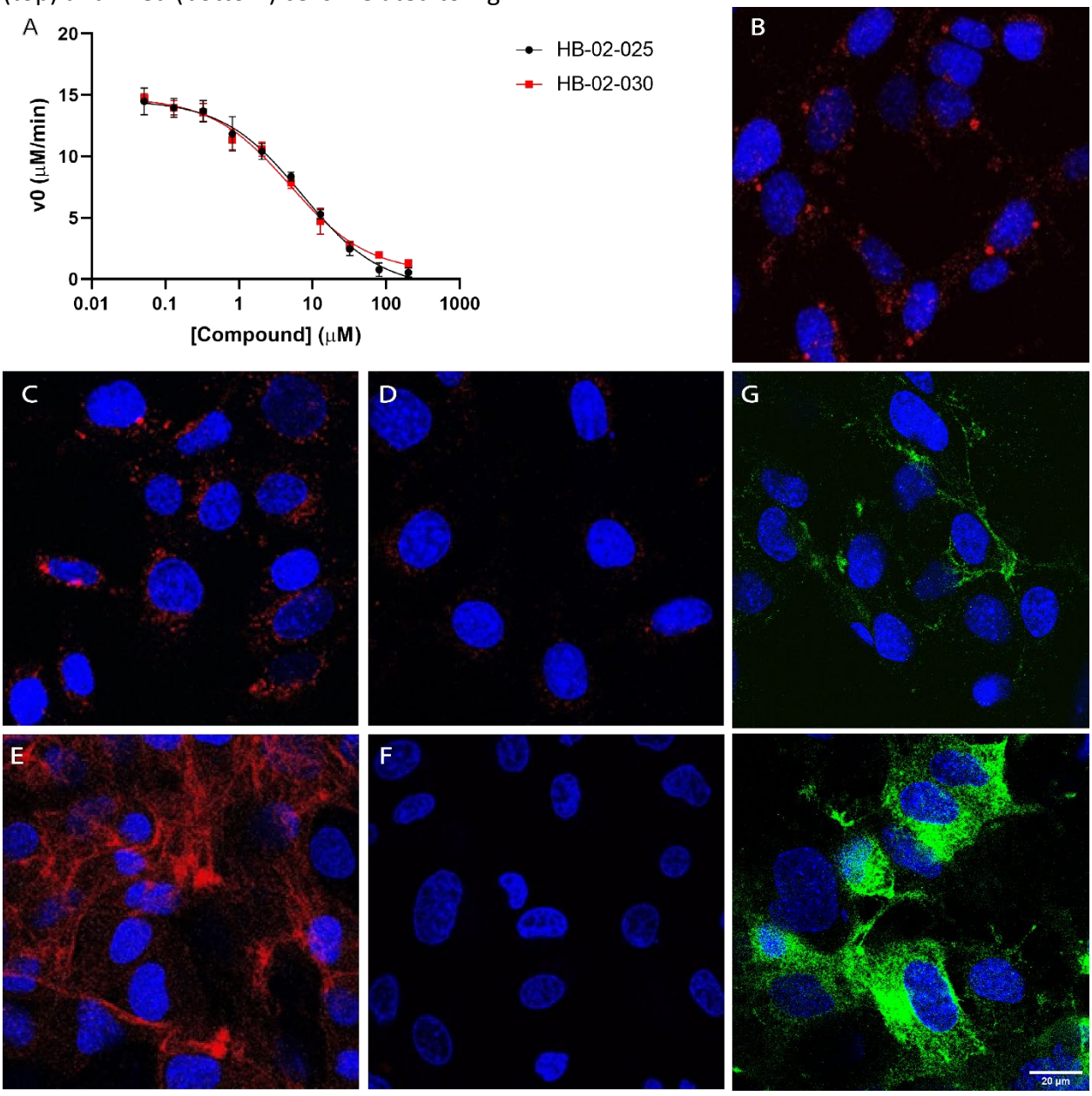

Figure S2: Wide plane views of panels in Fig. 2. Panel lettering and order is the same as in the main text figure. Related to Fig. 2.

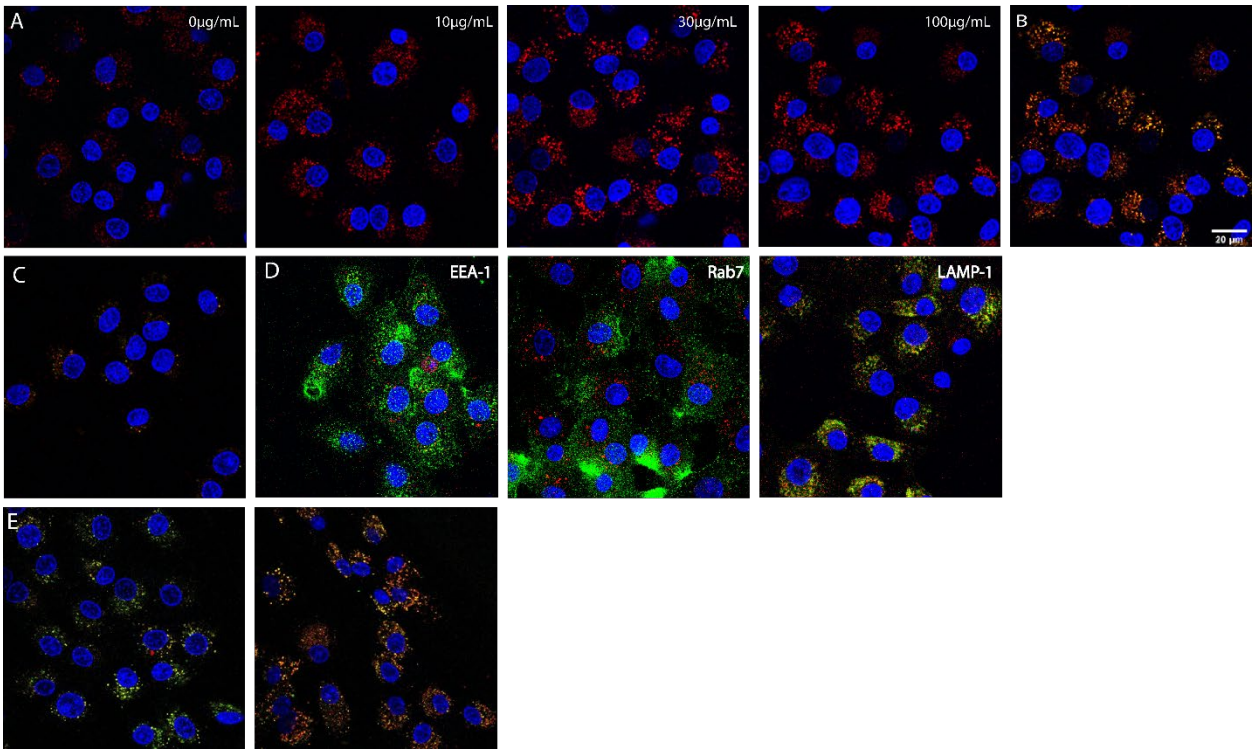

Figure S3: Multiple TG2 substrates, wide plan images of Fig. 3 panels. Panels (A) and (B); wide view of (A); show DP3-3, a potent TG2 inhibitor, having the same effect as HB225 causing endocytosis of α_2M. (C-F) Correspond to panels (B-E) of Fig 3. (G) Dose response to Cy5-33mer. (H) Dose response to fibronectin. Related to Fig. 3.

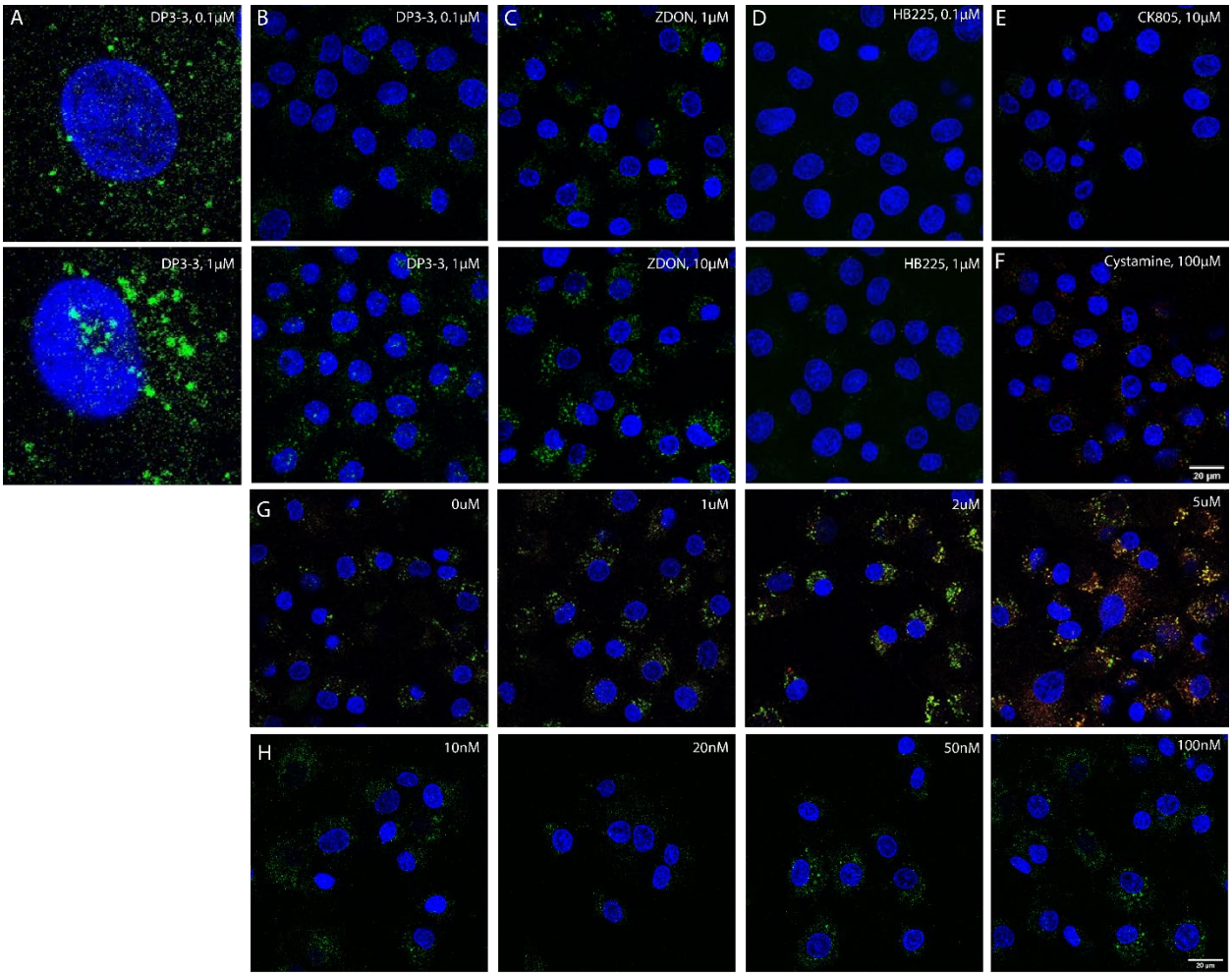

Figure S4: Kinetic analysis of TG2 and its truncated derivatives in the presence of α_2M. (A) When a gluten peptide mimic is used as a substrate, a significant decrease in k_{cat} is observed in the presence of α_2M. Inhibition is not observed when a lower affinity TG2 substrate is used (B). (C) Truncating TG2 by eliminating either one or both b-barels results in a loss of sensitivity to α_2M. TG2-Cb1 and TG2-Cb1-Cb2 correspond to derivatives lacking one or both C-terminal b-barrels of this four-domain protein. Relates to "Recognition of TG2 by α_2M" section and Fig. 3.

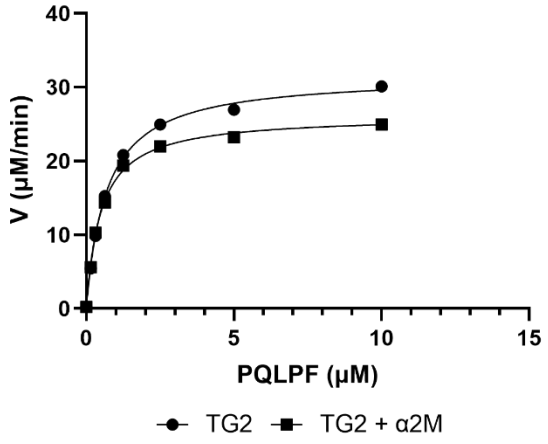

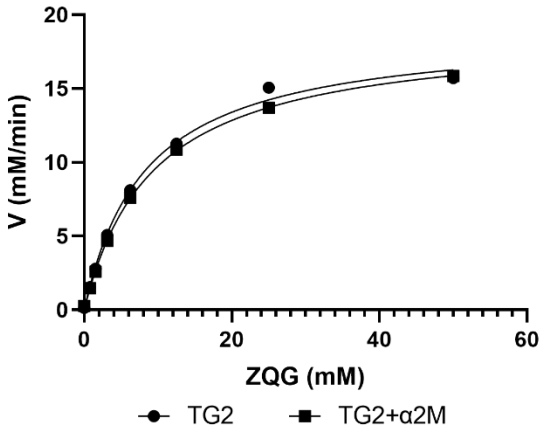

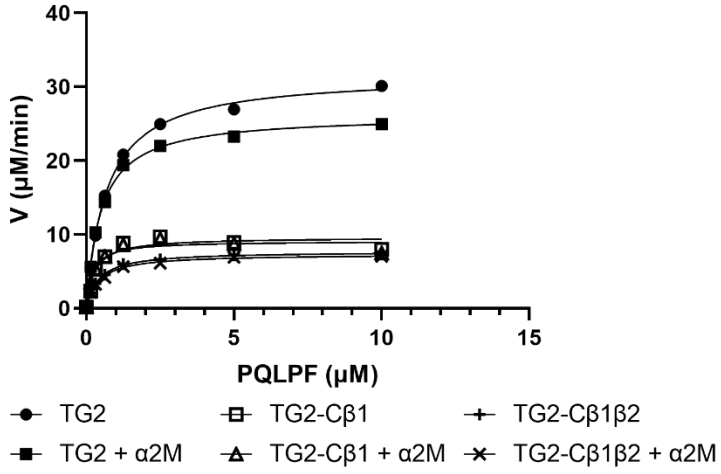

Table S1: Kinetic parameters for full length and truncated derivatives of TG2, with and without α_2M. Relates to "Recognition of TG2 by α_2M" section and Fig. 3.

TG2 derivative	**α_2M**	**kcat (min^{-1})**	**Km (µM)**
Full length	-	35.1 ± 1.2	0.68 ± 0.09
Full length	+	29.1 ± 1.0	0.50 ± 0.07
Lacking Cβ1	-	8.7 ± 1.4	0.27 ± 0.20
Lacking Cβ1	+	8.3 ± 1.1	0.20 ± 0.14
Lacking Cβ1 and β2	-	7.0 ± 0.19	0.41 ± 0.05
Lacking Cβ1 and β2	+	6.7 ± 0.31	0.41 ± 0.08

Figure S5: Wide view of images in panels (A-G) in Fig.4. Related to Fig. 4.

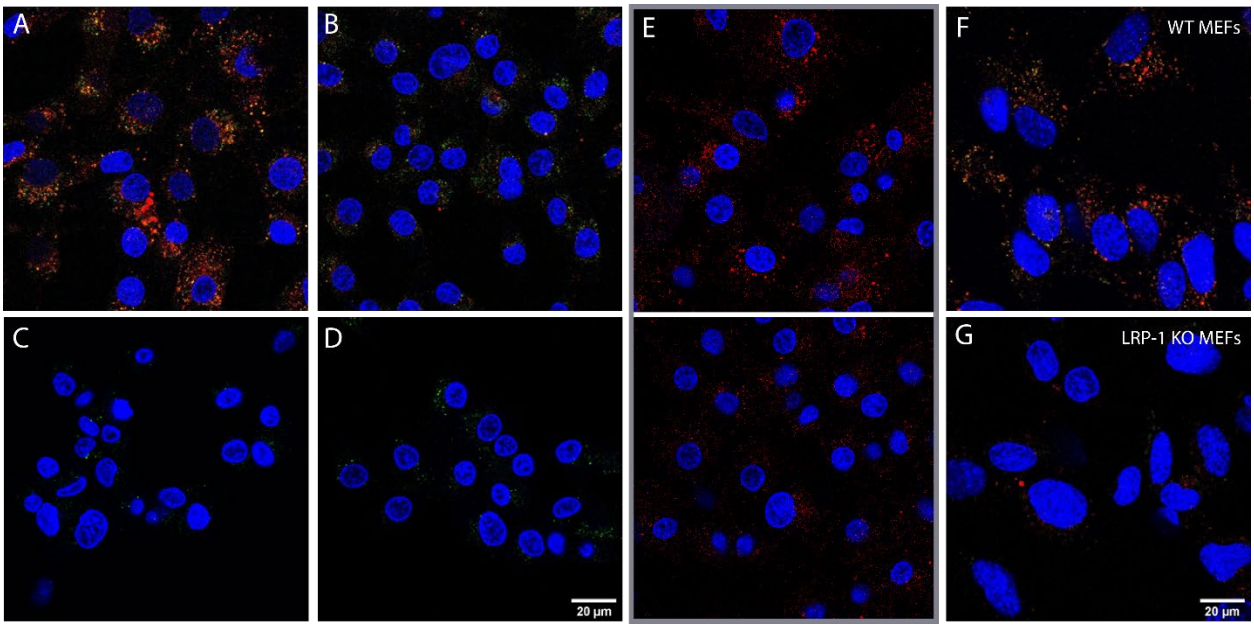

Figure S6: Wide view of images in Fig 5. (A) Dose response of 9022 cells to Pitstop. HB230 (B) and the deamidated 33mer (C) are not taken up in 9022 cells. Related to Fig. 5.

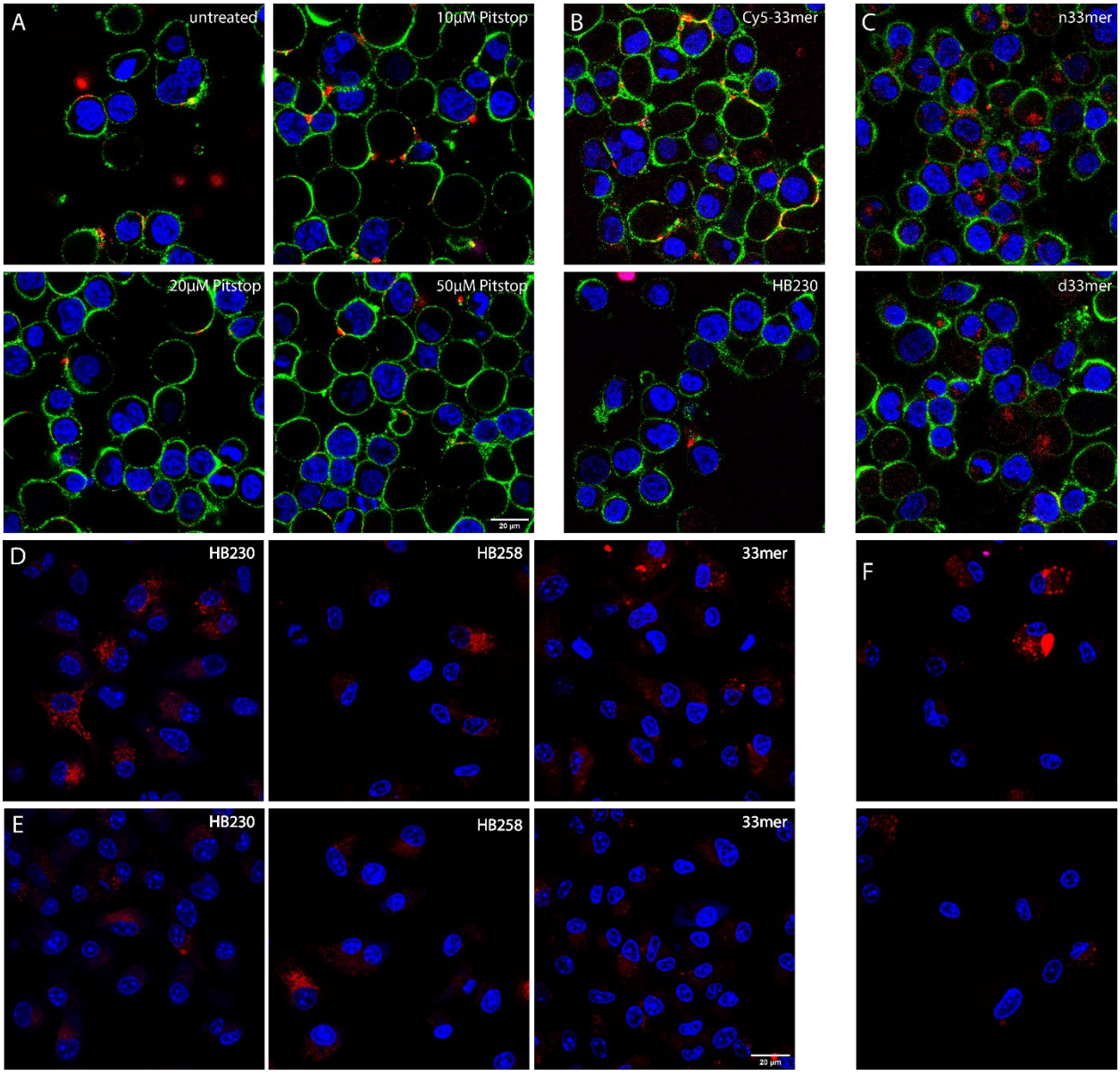

Figure S7: Expression of lrp1 in immune cells. (A) Macrophages, dendritic cells, and fibroblasts gene in the small intestine express the highest levels of the lrp1 gene. (B) Similarly, dendritic cells across all tissues express high levels of lrp1. Figures adapted from the ImmGen database (single cell RNAseq for the small intestine) and the Human Protein Atlas (Data from blood cells and PBMCs, (Monaco et al, 2019)). Related to Discussion section and Fig. 6.

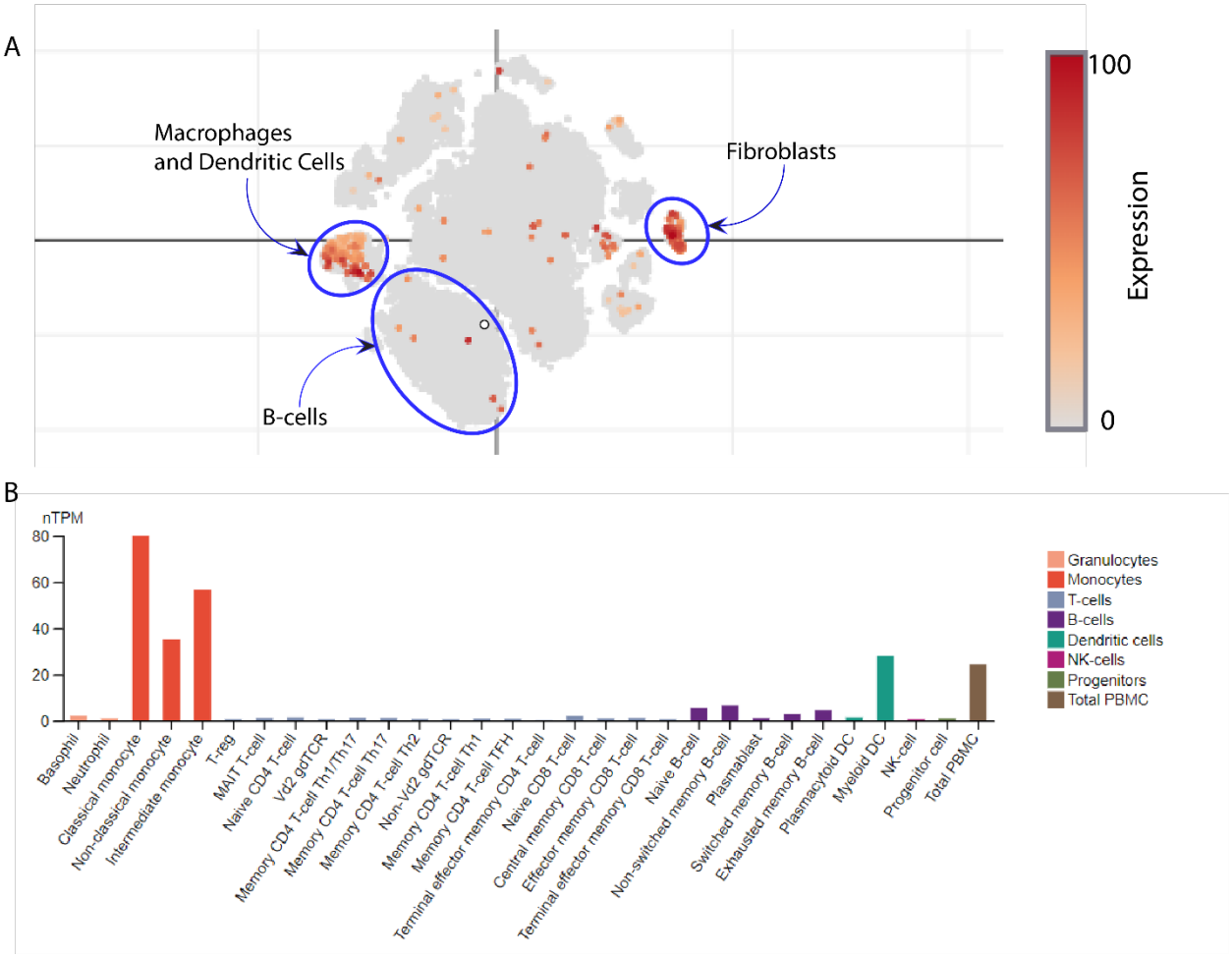

Data S1: NMR Spectra of intermediates and final products in the synthesis of the TG2 inhibitors used in this study. Related to Synthesis of Inhibitors section of the STAR Methods.

^{1}H NMR (400 MHz, $CDCl_3$) and ^{13}C NMR (101 MHz, $CDCl_3$) of **9**

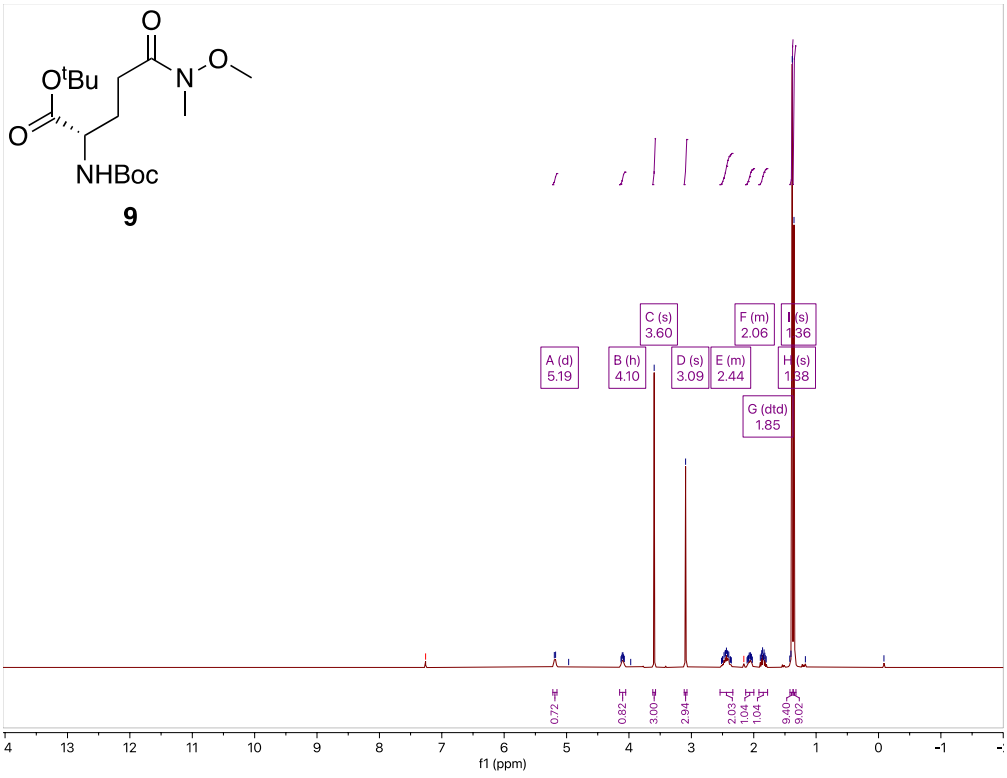

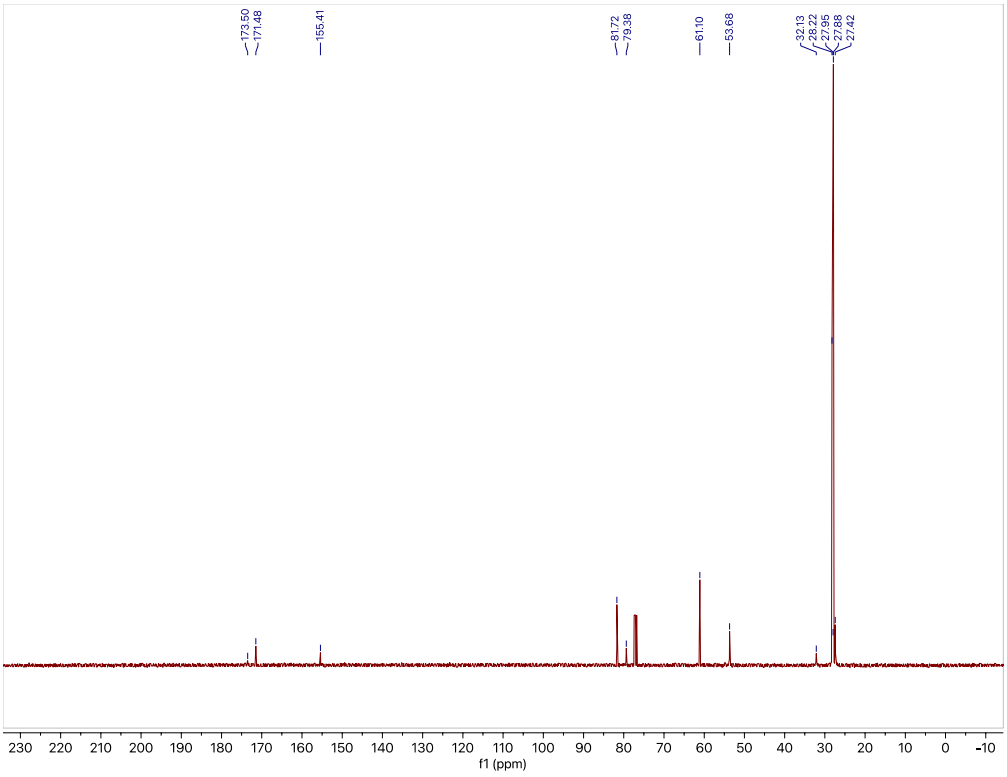

^{1}H NMR (400 MHz, $CDCl_3$) and ^{13}C NMR (101 MHz, $CDCl_3$) of **10**

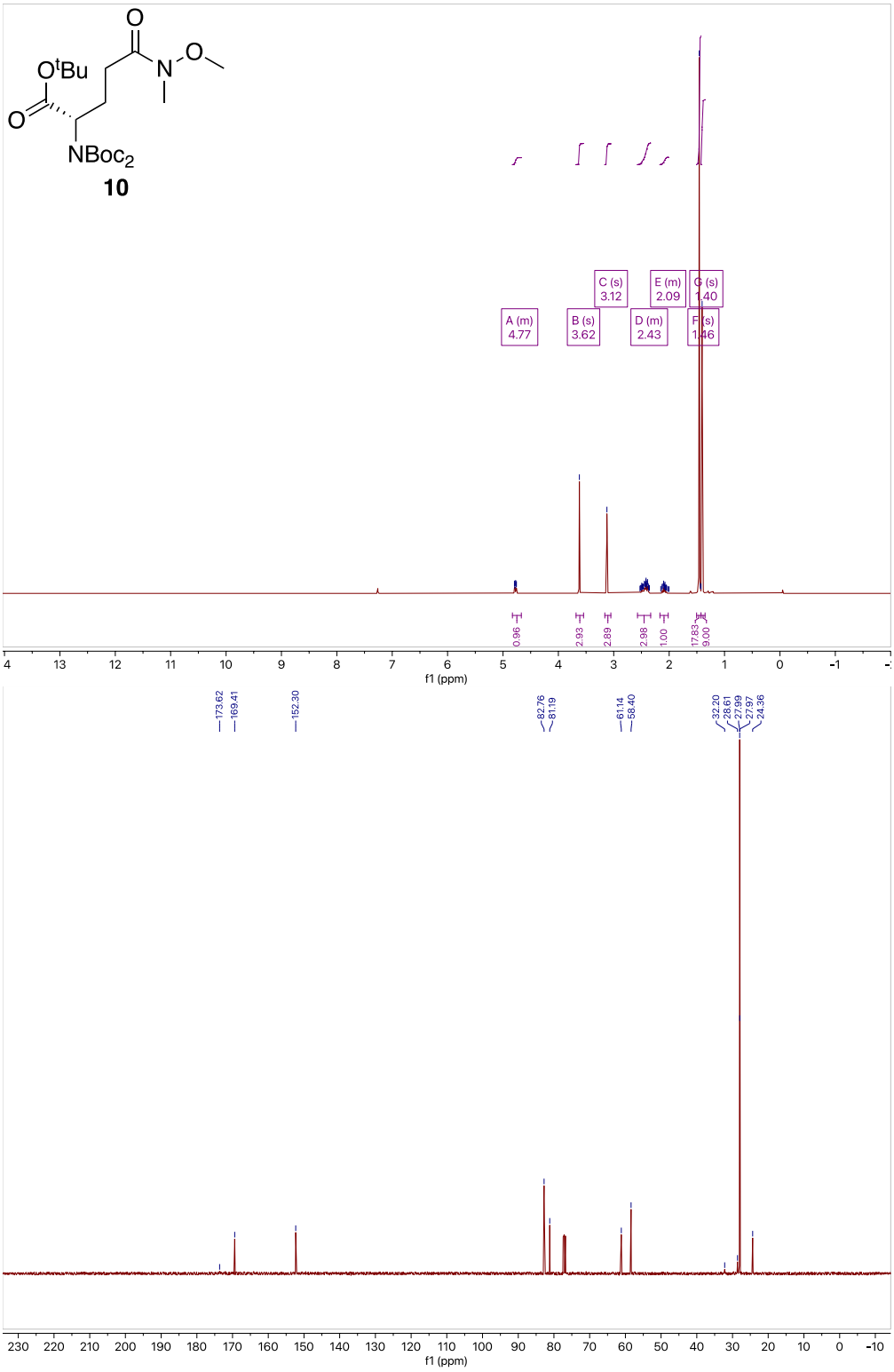

^{1}H NMR (400 MHz, $CDCl_3$) and ^{13}C NMR (101 MHz, $CDCl_3$) of **11**

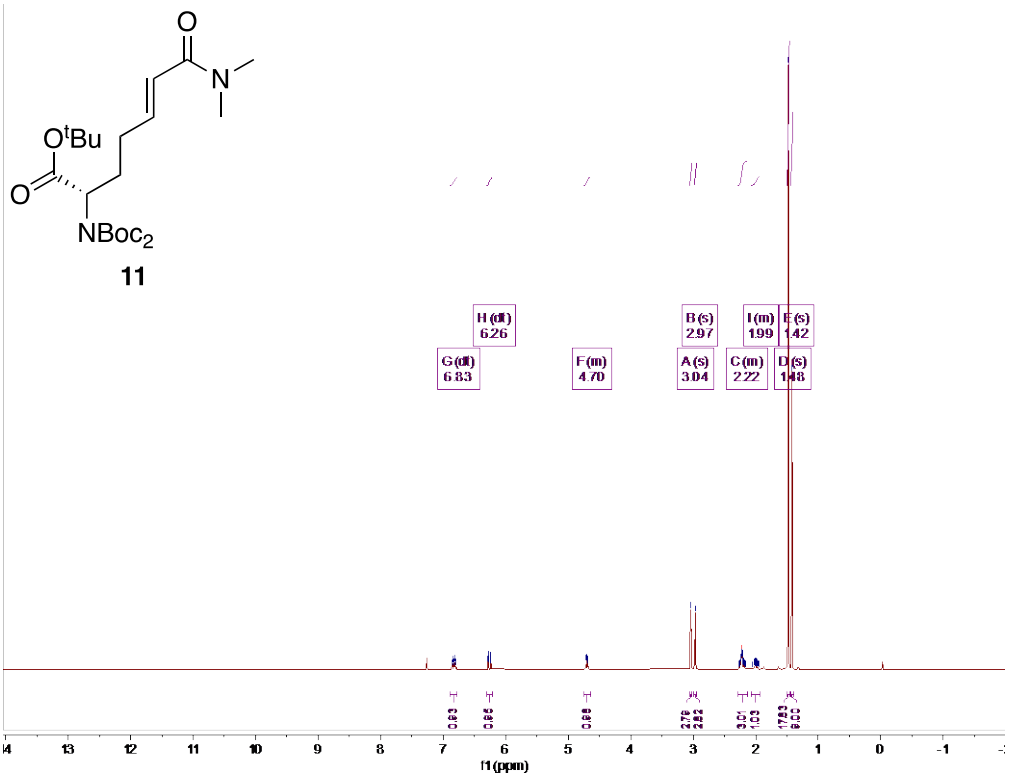

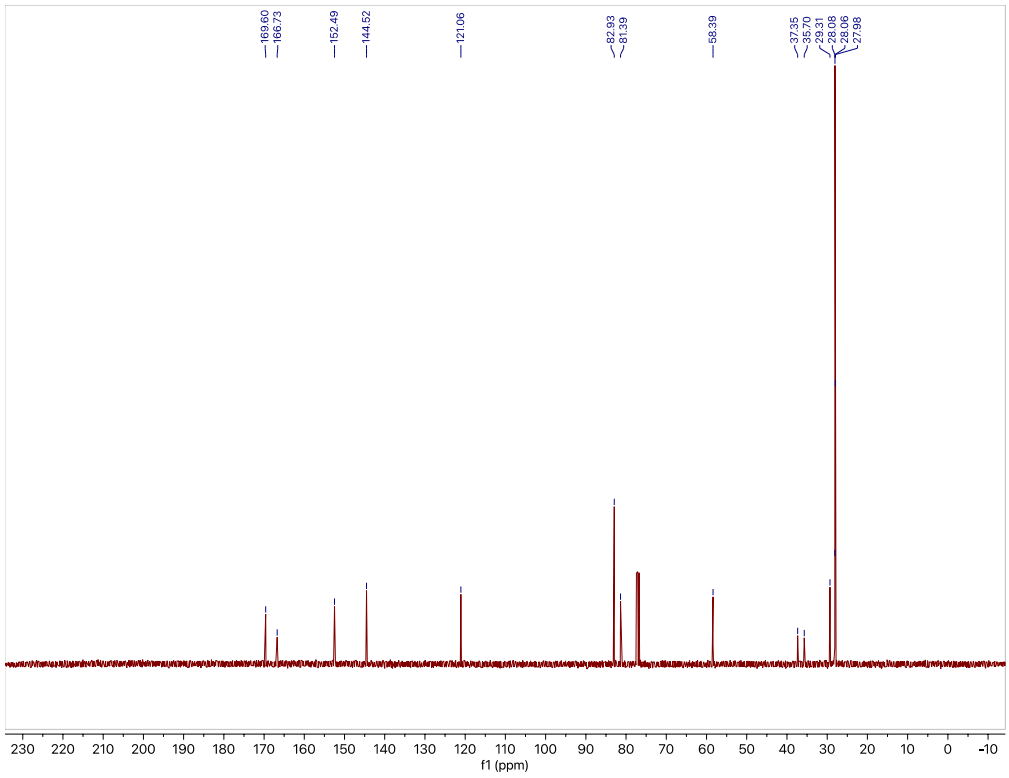

^{1}H NMR (500 MHz, DMSO-d_6) and ^{13}C NMR (126 MHz, DMSO-d_6) of **12**

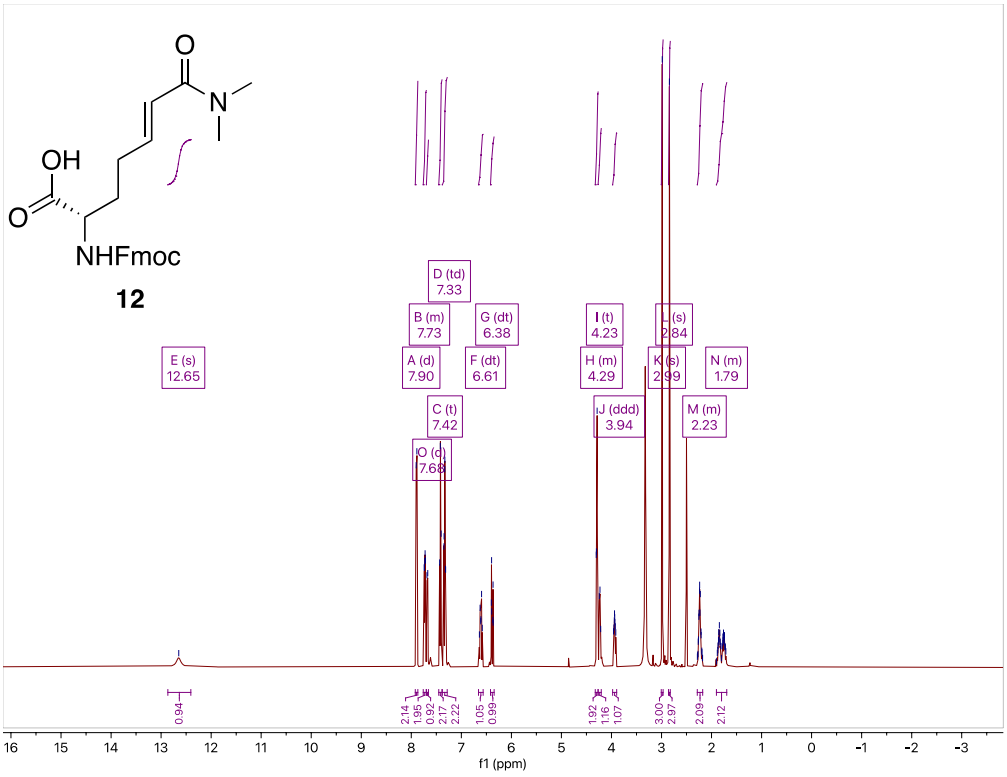

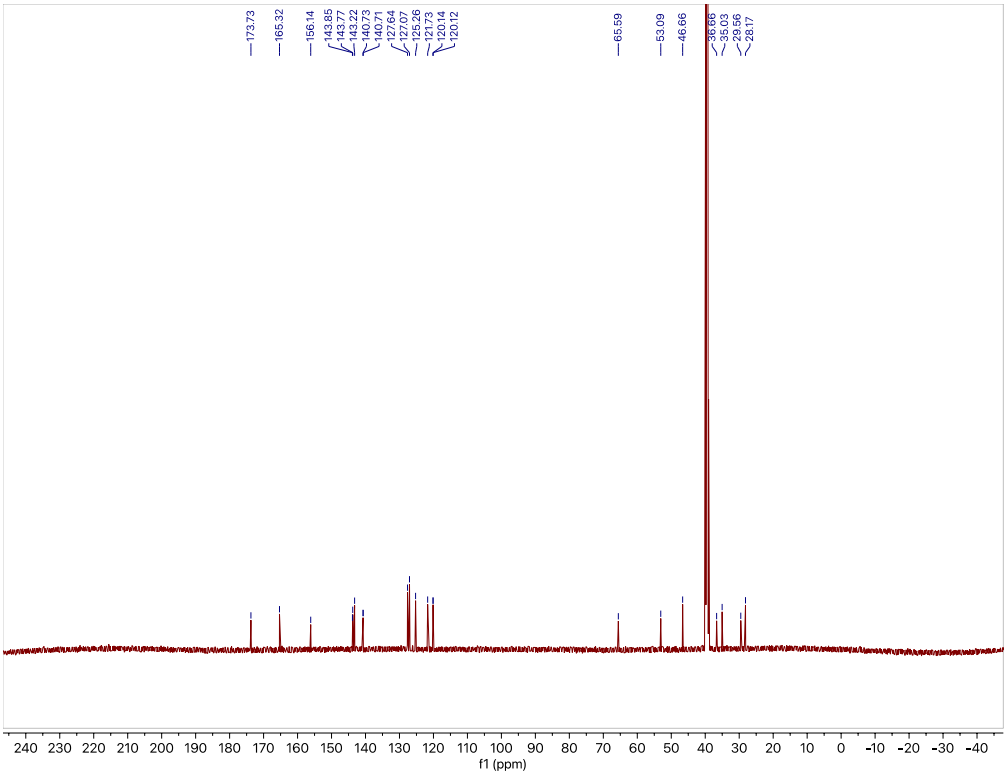

^{1}H NMR (500 MHz, $CDCl_3$) and ^{13}C NMR (126 MHz, $CDCl_3$) of **13**

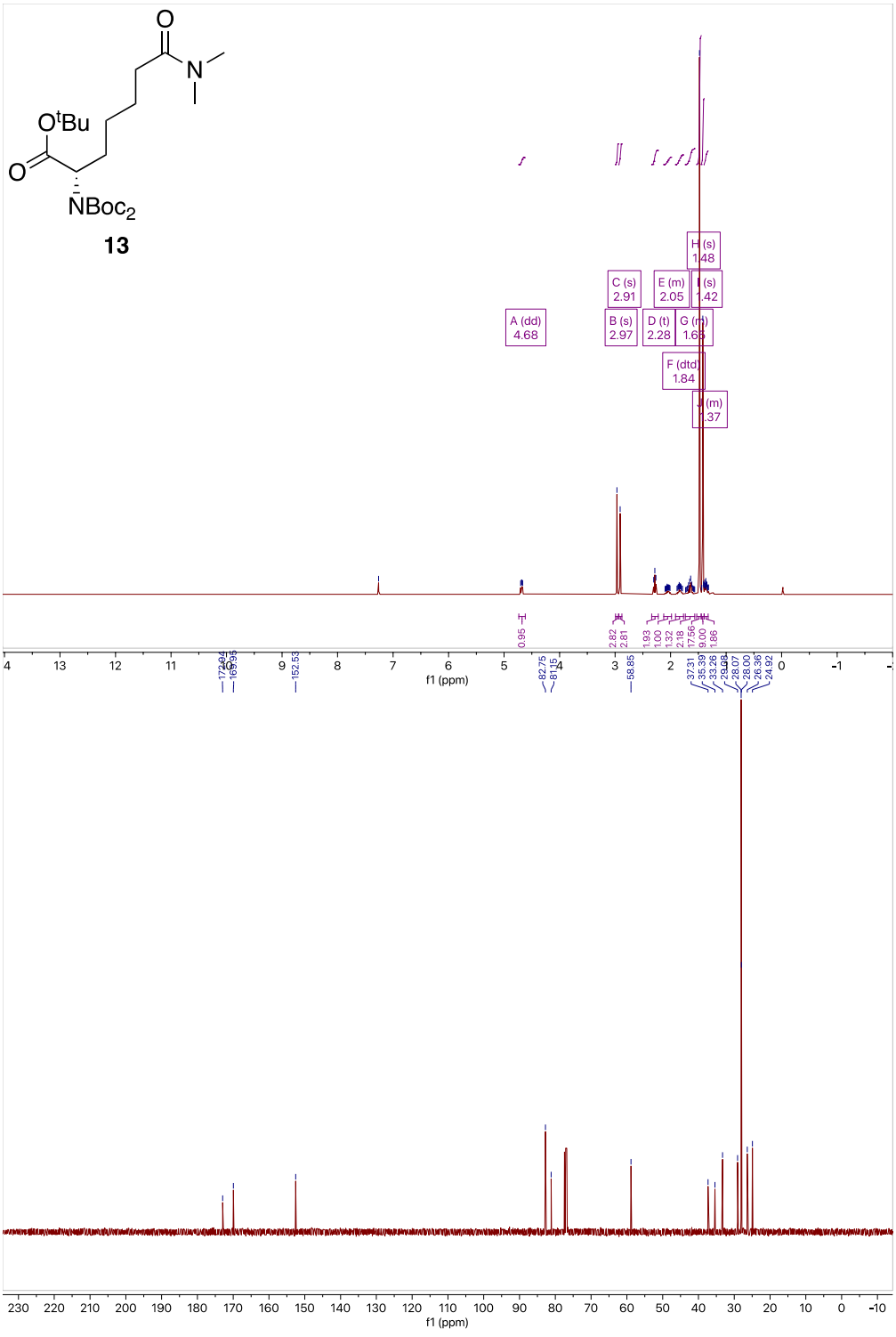

^{1}H NMR (500 MHz, DMSO-d_6) and ^{13}C NMR (126 MHz, DMSO-d_6) of **14**

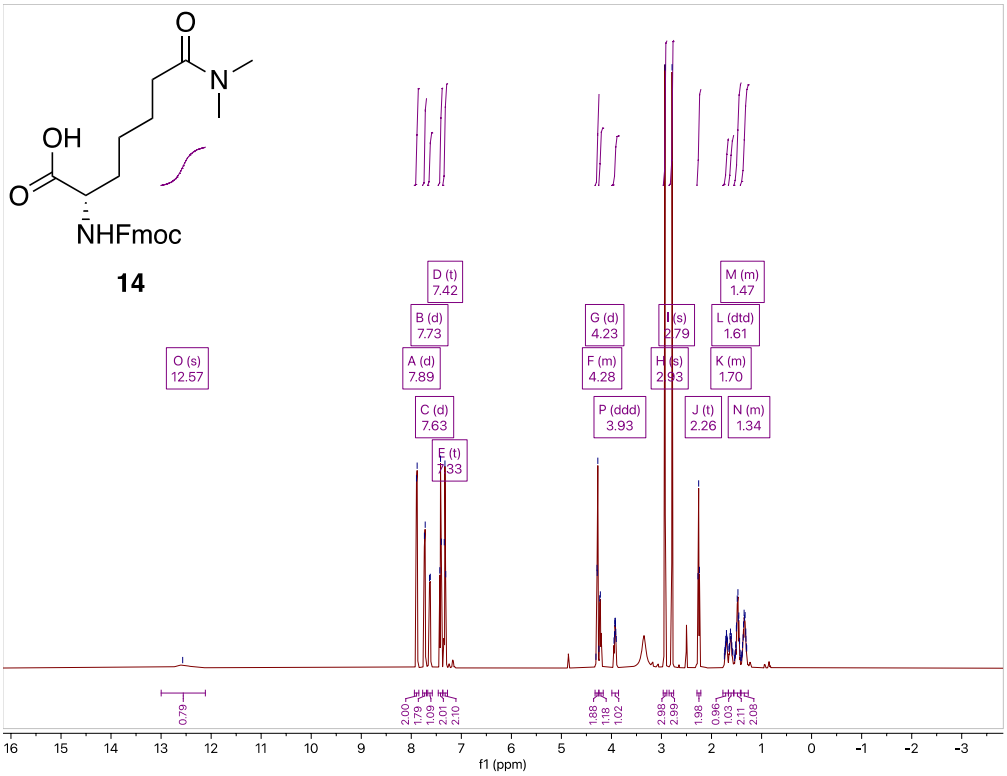

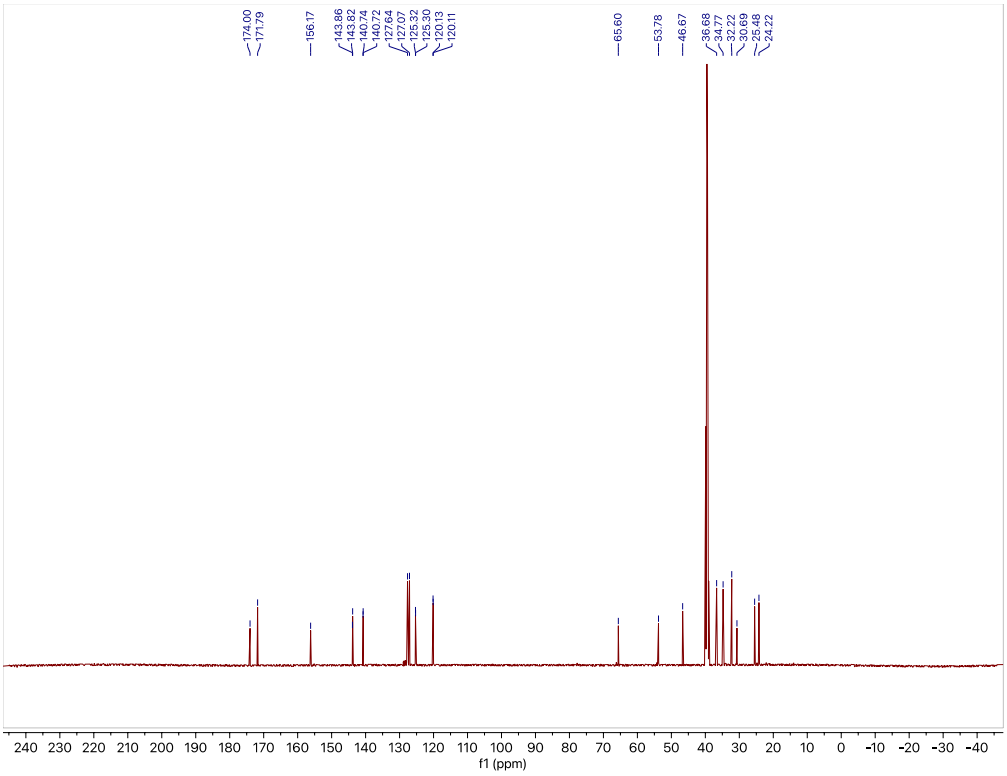

^{1}H NMR (500 MHz, $CDCl_3$), ^{13}C NMR (126 MHz, $CDCl_3$), and ^{31}P (202 MHz, $CDCl_3$) of **A**

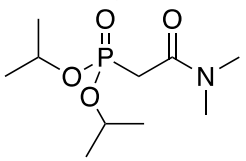

A

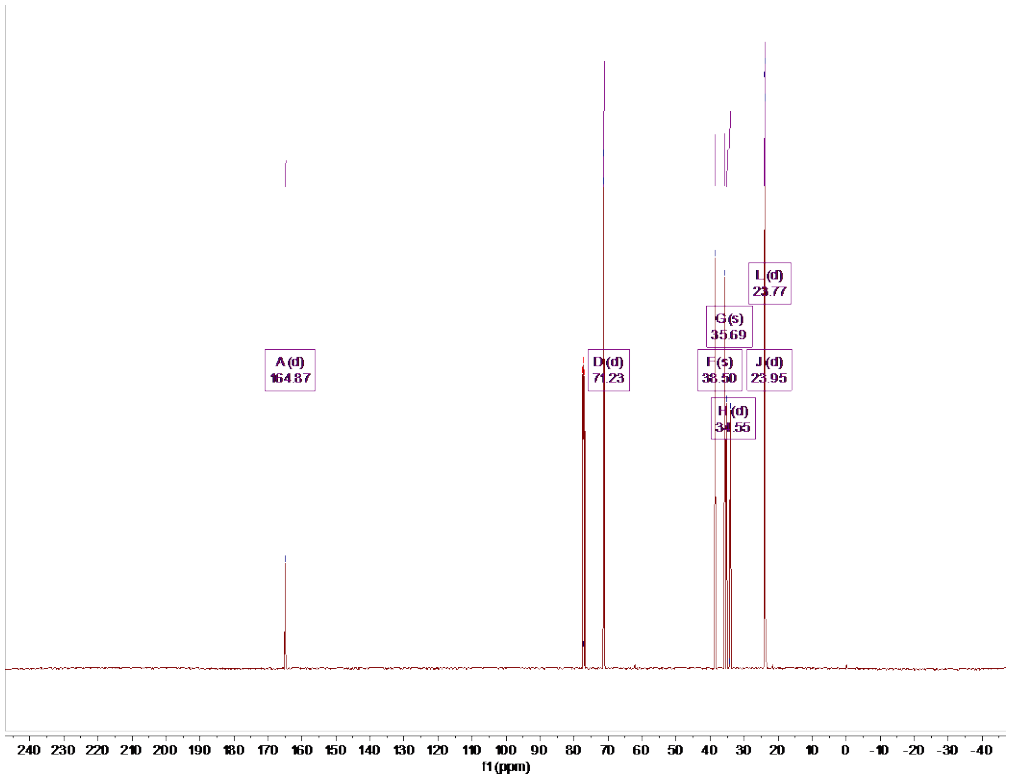

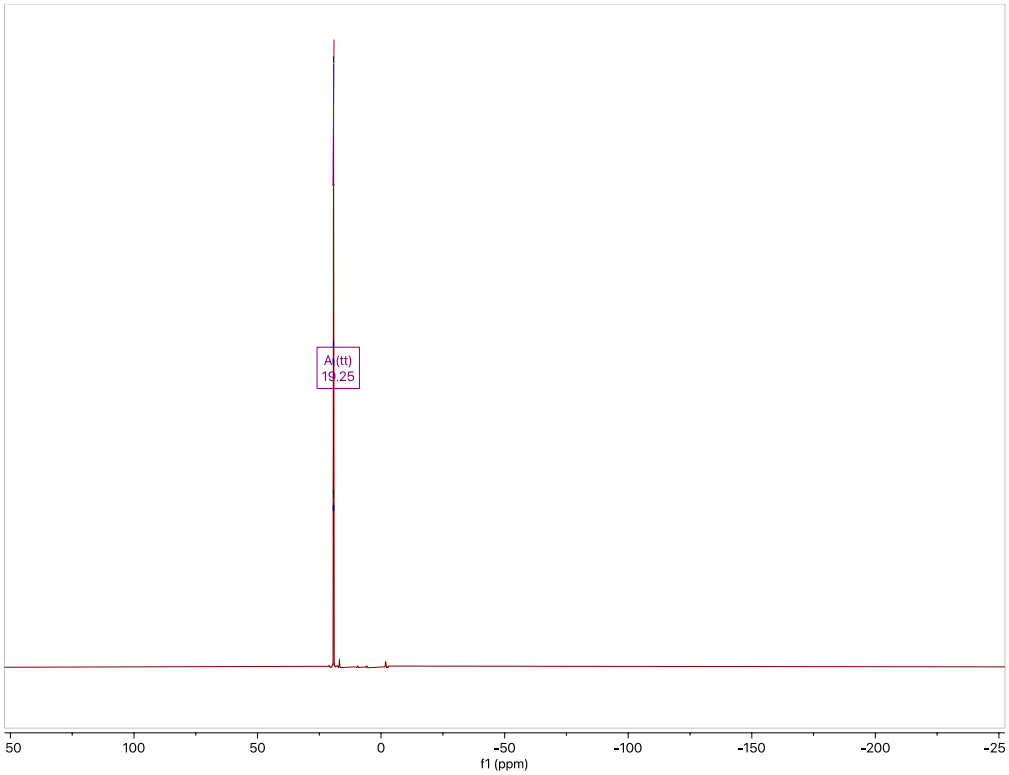

SI References

Monaco, G., Lee, B., Xu, W., Mustafah, S., Hwang, Y.Y., Carré, C., Burdin, N., Visan, L., Ceccarelli, M., Poidinger, M., Zippelius, A., Pedro de Magalhães, J. and Larbi, A. (2019). RNA-Seq Signatures Normalized by mRNA Abundance Allow Absolute Deconvolution of Human Immune Cell Types. *Cell Reports*, [online] 26(6), pp.1627-1640.e7. doi:10.1016/j.celrep.2019.01.041.